Available online at www.sciencedirect.com
ScienceDirect
Proceedings of the Combustion Institute 000 (2022) 1–9
Proceedings of the Combustion Institute
www.elsevier.com/locate/proci

Suppression of thermoacoustic instabilities by flame-structure interaction

Mariano Rubio-Rubio [a], Fernando Veiga-López [b], Daniel Martínez-Ruiz [c], Eduardo Fernández-Tarrazo [a], Mario Sánchez-Sanz [a,*]

[a] *Universidad Carlos III de Madrid, Av. de la Universidad 30, Leganés 28911, Madrid, Spain*
[b] *Institut Pprime, UPR 3346 CNRS, ISAE–ENSMA, BP 40109, Futuroscope-Chasseneuil Cedex 86961, France*
[c] *ETSIAE, Universidad Politécnica de Madrid, Madrid 28040, Spain*

Received 4 January 2022; accepted 19 July 2022
Available online xxx

Abstract

We present here an experimental study of the influence of the aeroelastic coupling between the combustion chamber walls and the acoustic fluid field on the onset and development of thermoacoustic instabilities in stoichiometric propane-air premixed flames. A horizontal quasi-two-dimensional Hele–Shaw chamber formed by two parallel plates separated a small distance h is used. The flames are ignited at the open end, in contact with the atmosphere, and propagate towards the opposite closed end. The experiments reveal three distinct propagation regimes determined by the stiffness of the plates and the evolution of the pressure perturbation generated during ignition: (i) for sufficiently rigid plates, we observed secondary acoustic instabilities with large amplitude oscillations in the direction of propagation of the flame; for flexible enough walls to be compliant with ignition-related pressure changes, (ii) the propagation of the flame undergoes small-amplitude oscillations (primary acoustic instabilities) along the channel or (iii) it is smooth with no oscillations whatsoever. The flexural rigidity of the plate is modified experimentally by changing both the width W and thickness h_w of the top plate of the Hele–Shaw cell. The data recorded by the pressure transducer and the accelerometer is used to plot a stability map in the $W - h_w$ parametric space to define the combination of structural parameters that triggers the onset of thermoacoustic instabilities. Our experimental measurements, supplemented with results from a theoretical analysis of the walls vibration modes, indicated that deformation-induced volume changes of around 0.1% of the volume of the Hele–Shaw cell are sufficient to suppress thermoacoustic instabilities.

Keywords: Thermoacoustic instabilities; Flame-structure interaction; Hele–Shaw cell; Premixed flames

* Corresponding author.
E-mail address: mssanz@ing.uc3m.es (M. Sánchez-Sanz).

https://doi.org/10.1016/j.proci.2022.07.165

1. Introduction

Thermoacoustic instabilities are oscillations that arise when the heat release rate of a system is coupled with its acoustic modes. In this study, a flame front reacts to an acoustic perturbation inside a semi confined combustion chamber. The unsteady pressure field induced by the flame creates a force on the walls of the vessel, introducing structural vibrations that can also interact with the gas mixture and modify the already complicated interplay between the flame and pressure waves. Previous experimental studies in quasi-2D configurations (e.g., Hele–Shaw cells) [1–4] considered wide flat plates to build the combustion chamber and study the onset and evolution of intrinsic hydrodynamic and thermo-diffusive flame instabilities without reporting significant pressure or flame oscillations during the experiments. On the other hand, the recent work by Veiga-López et al. [5,6] and Martínez-Ruiz et al. [7,8], among others, identified a regime of violent flame oscillations similar to those described by the seminal experiments in tubes by Searby [9].

Specifically, the interaction between the structural vibration and the flame instability was explored by Radisson et al. [10]. According to their results, the vibration of the plates was responsible for inducing oscillating instabilities in the flow field, which emerged from a direct coupling with the structural modes of the burner walls. The analysis therein proposed that the oscillation of the flow was induced by the burner natural vibration modes, introducing flame oscillation frequencies that did not agree with the prediction of characteristic frequencies in thermoacoustic instabilities. Very recently, Liu et al. [11] studied the effect of a flush-mounted flexible membrane over the duct wall on the suppression of unstable thermoacoustic modes. Using a numerical approach, the authors state that the thermoacoustic instability of the system can be controlled via vibro-acoustic coupling, concluding that this idea can be used as an effective control strategy by adjusting the physical parameters of the membranes and their installation locations.

Most importantly, numerous technological applications rely on the adequate prediction and control of this kind of processes to avoid structural failure and reduced efficiencies. The ability to control combustion-related instabilities might significantly reduce operational and maintenance costs, which can constitute up to 70% of the non-fuel costs of some turbines [12]. The understanding of mechanisms that avoid this problem will surely have a great impact on the performance and viability of power generation devices. Nevertheless, to the best of the authors' knowledge, the work by Pozarlik and Kok [13] is the only one that has considered the mutual interaction between flow, chemical reaction, acoustics and structural vibration in turbines to show that the vibration of the combustion chamber might play an important role to trigger or suppress thermoacoustic instabilities.

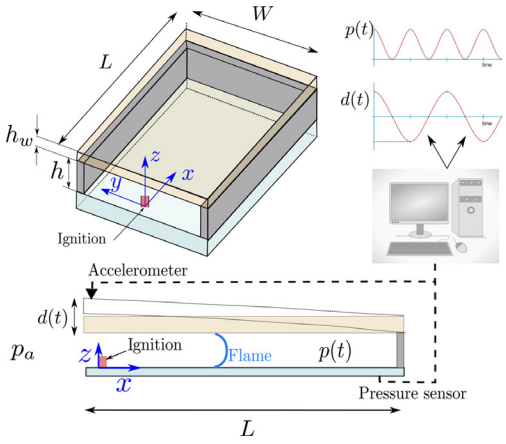

Fig. 1. Perspective (*top*) and side (*bottom*) view sketch of the experimental setup indicating the ignition point, accelerometer and pressure sensor. The distance between the plates h is much smaller than the width W and length L of the Hele–Shaw chamber $h \ll W \sim L$. The flame propagates from left to right towards the closed end of the chamber.

In this work, we present an experimental analysis under simplified geometries to explore the effect of the wall stiffness on the propagation of the flame. In the following sections we introduce a theoretical prediction linking the mechanical properties of the plates forming the Hele–Shaw chamber with the dynamics of the flame. Its influence on the coupling dynamics will be assessed in this paper to devise new methods to control and/or mitigate the onset of thermoacoustic instabilities.

2. Experimental setup and procedure

The experimental setup is sketched in Fig. 1 and thoroughly described in Veiga-López et al. [5]. The combustion chamber is formed by two flat plates disposed horizontally and separated by a PMMA hollow frame, enclosing a maximum volume of $L \times W \times h = 900 \times 500 \times 10\ \text{mm}^3$. The lower plate is a rigid aluminum table insulated with a 10-mm PVC layer at $z = 0$ mm. The top plate is a PMMA plate of width W, length L and thickness h_w, separated a distance h from the lower plate. During this study, L is kept constant, while the channel width W and the top-plate thickness h_w are modified to analyze the effect of the plates flexural rigidity on the propagation and acoustic coupling of propane flames.

The stoichiometric propane air mixture (equivalence ratio $\phi = 1$) is prepared before injection using two mass flow controllers (Sierra SmartTrak 100 for fuel and Omega FMA5418A, 0–5 slm for air). The experimental procedure starts by inject-

Please cite this article as: M. Rubio-Rubio, F. Veiga-López, D. Martínez-Ruiz et al., Suppression of thermoacoustic instabilities by flame-structure interaction, Proceedings of the Combustion Institute, https://doi.org/10.1016/j.proci.2022.07.165

ing the stoichiometric mixture into the chamber at the ignition end, via four regularly-spaced injection ports. During this phase, the ignition end of the vessel is kept sealed while the opposite end is opened for venting. Upon the completion of the charge, both ends are shut to allow the gases to come to rest. Finally, the ignition-injection end is reopened and the mixture is ignited using a glow plug (BOSCH Duraspeed) which produces the deposition of an electrical energy that is equal for all the experiments. The whole section $W \times h$ at the ignition end is available to freely vent the high-temperature products off the chamber.

The luminous emission of the flame is recorded with a high-speed camera (MEMRECAM HX-3) shooting between 1000 and 25,000 fps depending on the case. The top view (plane $x - y$ in Fig. 1) is used to obtain accurate quantitative data from the recording through the visually-accessible PMMA plates (i.e., oscillation frequencies, burned volume fraction, flame velocity, etc.). The front view (plane $y - z$ in Fig. 1) is used to visualize the interaction of the flame with the top plate right after ignition (see Fig. 6). Simultaneously, a pressure transducer located inside the chamber, near the closed end, is used to record the pressure signal $p(t)$ induced by the acoustic oscillations, with a characteristic sampling frequency of 6000 Hz. At the same time, an accelerometer measures the vertical acceleration of the top plate at the ignition point just above the glow plug. A low pass filter is applied to the acceleration signal to remove both mechanical and electrical noise, and a third-order time integration method is used to obtain the vertical displacement $d(t)$ from the data recorded by the accelerometer. Finally, image and signal post-processing analyses are performed using an in-house Python code.

In our experiments we describe the propagation of a flame that oscillates with a frequency f_f because of the interaction with an acoustic wave. The main contribution to the absorption of the sound wave is due to the presence of the walls, above which an acoustic boundary layer of thickness $\delta_v \sim (\nu/\pi f_f)^{1/2}$ accommodates the velocity oscillation amplitude of a fluid particle from its value in the mainstream to zero on the walls surface. As indicated in Landau and Lifshitz [14] for cylindrical pipes, the sound absorption coefficient decreases with the radius of the tube. In planar channels, Veiga-López et al. [5] demonstrated that a distance between the horizontal plates $h = 10$ mm is sufficient to make the viscous damping of the acoustic signal negligible.

3. Experimental results

The aforementioned methodology is applied here to obtain the following data on stoichiometric propane air mixtures. Three different regimes are identified from our experiments, two of them are illustrated in Fig. 2 and in the video attached as supplementary material. The figure shows a top-view image composition of the propagation of the flame from left to right, as recorded using rigid 25 mm-thick (upper half) and flexible 10 mm-thick (lower half) PMMA plates.

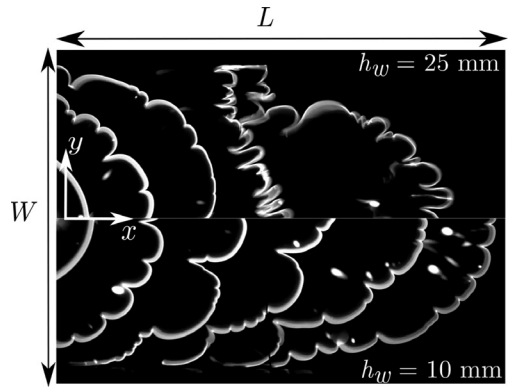

Fig. 2. Top view of the flame luminous emissions recorded by the high-speed camera at different times for $W = 500$ mm and $L = 900$ mm, with a 25 mm-thick PMMA plate (upper half) and a 10 mm-thick PMMA plate (lower half).

In the case illustrated in the upper half of Fig. 2 (thicker plate), the stoichiometric flame wrinkles to form medium-size cells, as a consequence of the Darrieus Landau instability, short after the ignition event. Later, the flame starts a small-amplitude oscillation that flattens the reacting front before reaching the first quarter of the chamber. Following that phase, when the reactive front progresses towards the half of the chamber, the oscillations grow rapidly in amplitude up to 6000 Pa (see top panel of Fig. 3), accelerating the flame. It is at this point that the front adopts a marked cellular finger-like shape, that simultaneously alternates cusps and tails in consecutive periods. This is the characteristic behavior of premixed flames undergoing secondary acoustic instabilities that exhibit large-amplitude oscillatory dynamics.

When the thickness of the plate is progressively reduced, the amplitude of flame oscillations becomes smaller, propagating with primary thermoacoustic oscillations for 10 mm $< h_w \leq$ 20 mm, not shown here for the sake of conciseness. Given $h_w \leq 10$ mm, no flame oscillations are observed. The particular case of $h_w = 10$ mm is shown in the lower half of Fig. 2. In this experiment, the flame initially developed the characteristic Darrieus-Landau wrinkling but the evolution was smooth with nearly-constant flame propagation velocity and no oscillations of the reacting front.

The pressure history $p(t)$ and the vertical displacement of the upper plate $d(t)$, obtained

Please cite this article as: M. Rubio-Rubio, F. Veiga-López, D. Martínez-Ruiz et al., Suppression of thermoacoustic instabilities by flame-structure interaction, Proceedings of the Combustion Institute, https://doi.org/10.1016/j.proci.2022.07.165

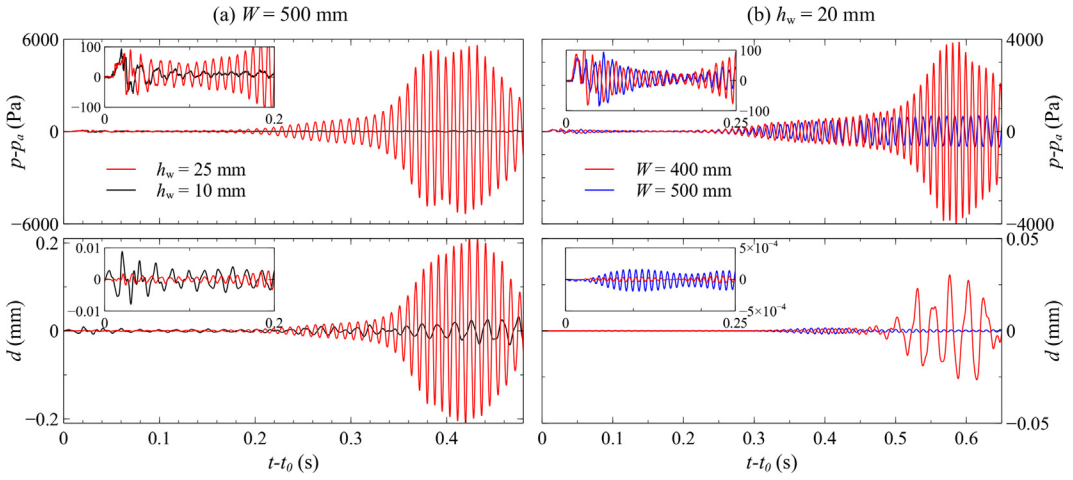

Fig. 3. Pressure $p - p_a$ (top) and displacement d (bottom) evolution with time $t - t_0$ for a) two different top-plate thicknesses, $h_w = 25$ mm (red) and $h_w = 10$ mm (black) with $W = 500$ mm and b) two different top-plate widths, $W = 400$ mm (red) and $W = 500$ mm (blue) with $h_w = 20$ mm. The insets in the figures show the initial instants of $p - p_a$ and d after the ignition event at $t = t_0$. (For interpretation of the references to color in this figure legend, the reader is referred to the web version of this article.)

through the pressure transducer and accelerometer respectively, are both shown in Fig. 3(a) for $W = 500$ mm, $L = 900$ mm and different plate thicknesses. When a thick plate of $h_w = 25$ mm was used, the pressure history corresponds to the classical pattern of secondary instabilities mentioned above and reported before in Veiga-López et al. [5], Searby [9]. The time history of the vertical displacement $d(t)$, shows an identical shape to that of the pressure record, with a maximum displacement of around 0.2 mm and an oscillation frequency of $f_f = 114$ Hz. Nevertheless, the use of a plate of $h_w = 10$ mm produces a change in the behavior, making the pressure oscillations disappear. The effect of the variation of the channel width W on the pressure and displacement response is shown in Fig. 3(b). In this figure, we identify a similar effect to reduce the plate thickness, with a transition from secondary to primary thermoacoustic instabilities when the chamber width is increased from $W = 400$ mm to $W = 500$ mm. The measured flame oscillation behaviour (secondary, primary or no-oscillation) and the oscillation frequencies in terms of W and h_w are included in Table 1 in the Appendix.

Although the ignition of the flame caused the initial displacement of the top plate, we need to determine if the subsequent motion depends only upon the inherent properties of the system (natural oscillations) or, in contrast, is driven by pressure oscillations generated by flame instabilities. With that objective in mind, the following section is devoted to describe the structural properties of the plate and to calculate of the plate's natural oscillation frequencies.

4. Structural considerations

The structural properties and boundary conditions of the upper plate are a key point to devise the influence of the structure on the thermoacoustic coupling. As defined in the experimental set-up, the lower plate is attached to a solid aluminium table that can be considered infinitely rigid as $(Eh_w^3)_{Al}/(Eh_w^3)_{PMMA} \sim 35 \gg 1$. The upper plate, on the other hand, is a transparent PMMA rectangular plate where the three edges corresponding to the closed sides shown in the sketch included in Fig. 1 are clamped. The edge on the open end is free of any restriction. The frequency values associated to those specific constraints can be obtained using the semi-analytical method described in Leissa [15]. Nevertheless, and to avoid the uncertainties of the semi-empirical parameters used in this reference, the natural oscillation frequencies of the top plate were numerically calculated, using standard Finite Element Method techniques in Comsol Multiphysics, for the first and second deformations modes. The values of W, L and h_w in these calculations correspond to those used in the experiments. The values of the Youngs Modulus $E = 1934$ MPa and Poissons ratio $\nu = 0.33$ for the PMMA plates used in our measurements were gauged in our laboratories to ensure the maximum possible accuracy in the calculations of the natural frequencies. In particular, for a plate of width $W = 500$ mm, length $L = 900$ mm and thickness $h_w = 25$ mm, the fundamental frequency obtained for the first deformation mode is $f_p = 142.7$ Hz. The complete set of computations for all the range of parameters W and h_w considered are included

Please cite this article as: M. Rubio-Rubio, F. Veiga-López, D. Martínez-Ruiz et al., Suppression of thermoacoustic instabilities by flame-structure interaction, Proceedings of the Combustion Institute, https://doi.org/10.1016/j.proci.2022.07.165

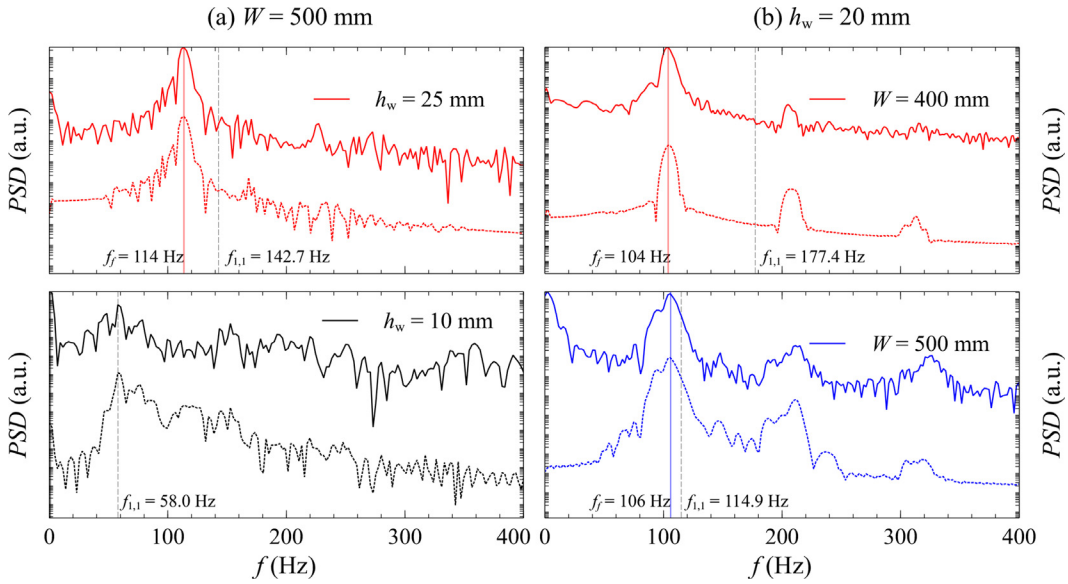

Fig. 4. Frequency analysis of both pressure (solid) and displacement (dashed) signals in the cases a) $W = 500$ mm with $h_w = 25$ mm (secondary thermoacoustic instabilities) and $h_w = 10$ mm (no pressure oscillations) and b) $h_w = 20$ mm with $W = 400$ mm (secondary thermoacoustic instabilities) and $W = 500$ mm (primary oscillations). The colored vertical lines indicate the pressure or flame frequencies f_f, while the dashed, gray lines show the natural frequency of the plate $f_{1,1}$ for each case.

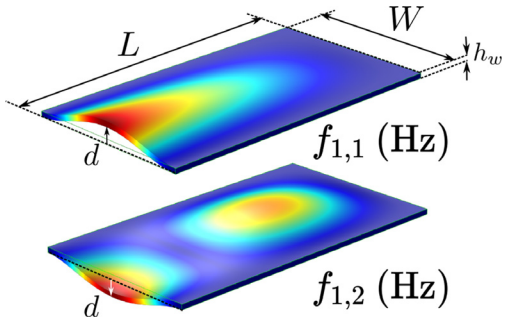

Fig. 5. First (top) and second (bottom) deformation modes of the plate. The natural frequencies of both deformation modes are included in Tables 2 and 3 in the Appendix.

in Tables 2 and 3 in the Appendix for the first and second deformation modes, respectively, which are illustrated in Fig. 5. In the former, the shaded region corresponds to those cases in which secondary flame oscillations were experimentally observed.

The frequency analyses of the flame oscillation, pressure and plate displacement signals are plotted in Fig. 4. As shown in this figure, for $W = 500$ mm and $h_w = 25$ mm we find a coherent peak at $f_f = 114$ Hz but not at $f_p = 142.7$ Hz, suggesting that the vibration of the plate is induced by the acoustic pressure wave travelling inside the channel, whose frequency only depends on the geometrical details of the Hele–Shaw cell and the properties of the gas. A similar behavior is observed with different combination of parameters. Nevertheless, we found a controversial case when $h_w = 20$ mm and $W = 500$ mm. In that experiment, the flame oscillation frequency $f_f = 106$ Hz is sufficiently close to the natural frequency of the plate $f_{1,1} = 114.9$ Hz to raise suspicion about the real origin of the oscillations observed in the experiments. Nonetheless, as the chamber width was reduced to $W = 400$ mm, keeping $h_w = 20$ mm, the flame oscillation frequency remained constant at $f_f = 104$ Hz but $f_{1,1} = 177.4$ Hz, sufficiently larger than f_f to confirm the pressure coupling as the real cause of the oscillations.

In addition, when the plate is under the effect of an uniformly distributed constant load of intensity $\mathcal{P}$, the vertical displacement of the plate d relative to the channel height h can be explicitly calculated [16] as

$$\frac{d}{h} = \Lambda \mathcal{H}(x, y)\mathcal{P}, \tag{1}$$

where $\Lambda = 12(1 - \nu^2)W^4/(Eh h_w^3)$ is the rigidity factor, and $\mathcal{H}(x, y)$ is a known periodic function that only depends on geometrical parameters It can be written as an infinite series of sines and cosines and ensures the boundary conditions of zero vertical displacement at $y = \pm W/2$ and $x = L$. Therefore, Eq. (1) anticipates the parametric dependence of the deformation of the vibrating plate with the

Please cite this article as: M. Rubio-Rubio, F. Veiga-López, D. Martínez-Ruiz et al., Suppression of thermoacoustic instabilities by flame-structure interaction, Proceedings of the Combustion Institute, https://doi.org/10.1016/j.proci.2022.07.165

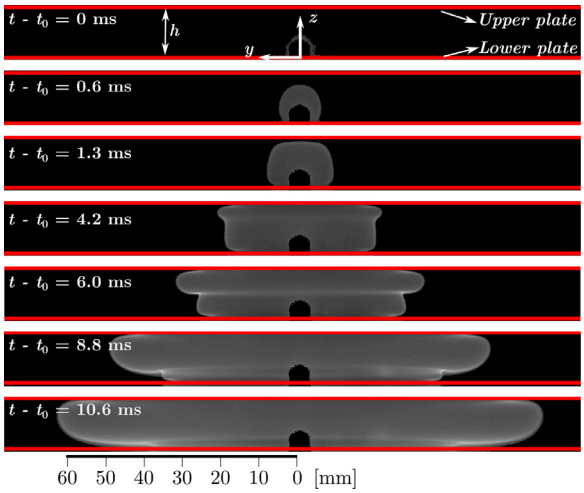

Fig. 6. Frontal view of the first instants of flame propagation near the glow plug located at $y = z = 0$ mm.

geometrical details through the stiffness coefficient Λ.

Unexpectedly, the vertical displacement of the top plate is reduced one order of magnitude when $h_w = 10$ mm, although the same material for the horizontal plate is used in our experiments. As seen through the flame front in Fig. 2 (lower half) and the pressure record in Fig. 3(a) (black curves), both pressure and flame front oscillations completely disappear. The maximum pressure increase in this case was around 100 Pa, a value significantly below the 6000 Pa recorded in the previous case with $h_w = 25$ mm, and of the same order as the over pressure generated during ignition (see inset in Fig. 3). The evaluation of the natural frequency of the PMMA plate with this $h_w = 10$ mm provides $f_p = 58$ Hz. In this precise experiment (Figs. 3 and 4), we observed a peak at this frequency in the displacement signal, but not in the pressure, clearly indicating that the vibration of the plate does not induce flame oscillations.

5. Discussion

To gain further insight into the thermal and structural nature of the observations, this section is devoted to study the physical mechanisms driving the experimental measurements. First, we explore the details of the evolution of the flame propagation right after ignition in Fig. 6. To take this sequence of images, the high-speed camera is placed horizontally at the open end of the chamber and set to record at 15,000 fps, focusing at the ignition in the $y - z$ plane. During the post-processing of the footage, the glow plug luminosity at $y = z = 0$ was removed for an improved visualization. The evolution of the front illustrates how the over pressure measured by the pressure transducer is built once the flame hits the upper plate of the Hele–Shaw chamber. Once this happens at approximately $t - t_0 = 1.3$ ms, with t_0 representing the ignition time, pressure increases locally near $z = h$, and the flame starts propagating faster in the proximity of the upper wall. That event creates an axisymmetric bulge in the reaction front, readily noticeable at $t - t_0 = 6$ ms, which then grows to overcome the slower region of the reactive front that moves close to the lower plate at $z = 0$ mm. Finally, at $t - t_0 = 10.6$ ms, a single parabolic-like flame propagates towards the sides of the chamber.

In addition, both the pressure and plate displacement signals shortly after ignition were given in the insets of Fig. 3. As a consequence of the initiation of the chemical reactions, a pressure rise of around 100 Pa is created when $W = 500$ mm and $h_w = 10$ mm. For estimation purposes, that pressure applied to the 0.5 m^2 plate gives a vertical force of the order of 50 N that deforms the upper plate producing a small volume change. If the plate is sufficiently rigid, the deformation is negligible and the initial pressure wave created during the ignition becomes trapped between the flame and the closed end of the Hele–Shaw cell. As demonstrated in Veiga-López et al. [5], Martínez-Ruiz et al. [8] for propane flames, under the conditions of our experiments, this acoustic wave would couple with the flame triggering the onset of thermoacoustic instabilities illustrated in Figs. 2 and 3. On the other hand, compliant walls with less flexural rigidity will suffer initially a greater vertical displacement that, in turn, induces a pressure change that can be estimated using the ideal gas equation to give $\Delta p/p = -\Delta V/V \sim -d/h$. According to Eq. (1), once the properties of the material are chosen, this ratio of vertical displacement of the plate d/h is controlled by the width W and thickness of the plate h_w. More precisely, the controlling parameter

Please cite this article as: M. Rubio-Rubio, F. Veiga-López, D. Martínez-Ruiz et al., Suppression of thermoacoustic instabilities by flame-structure interaction, Proceedings of the Combustion Institute, https://doi.org/10.1016/j.proci.2022.07.165

is identified to be the stiffness coefficient Λ defined above.

Even though the dynamical load created by the flame ignition is not uniform and the response of the plate will be different to that anticipated in Eq. (1), it is possible to use the scaling suggested by this equation to vary the rigidity of the upper plate, thus controlling the amplitude of the plate vertical displacement. Therefore, the same material for the top plates is maintained while varying the thicknesses h_w and widths W to keep constant both Poisson's ratio ν and Young's modulus E.

The set of experiments performed in our setup shows a systematic shifting of the flame frequency towards lower values as the thickness of the plate is reduced, giving, for example $f_f = (114, 106, 100)$ Hz for $h_w = (25, 20, 15)$ mm in a plate of width $W = 500$ mm. As the thickness is reduced, the plate becomes more flexible and the distance between the horizontal plates increases a small quantity d as a consequence of the overpressure Δp built during the propagation of the flame. The relative change of volume d/h, of the order of 0.1% of the chamber volume, increases with the overpressure and is inversely proportional to E and h_w so that $d \propto \Delta p/(h_w E)$ [17]. This slight volume expansion, in turn, reduces the pressure level, the velocity of the acoustic wave traveling in the chamber and, therefore, the amplitude and oscillation frequency of the flame.

Once the structural aspects of the experiments have been discussed, we turn our attention now to the influence of heat losses on our measurements. The sensibility of the acoustically-induced flame oscillation to heat losses has been recently addressed by Flores-Montoya et al. [18]. Varying the wall temperature, they showed that heat losses to the walls change the interplay between the acoustic field and the reaction sheet, diminishing the oscillation frequency of flames affected by thermoacoustic instabilities in tubes.

This effect, that will be present in our case as well, only depends on the unburned gas temperature, which is the same in all cases tested here. Nevertheless, reducing h_w might eventually have an effect on the flame propagation speed as a consequence of the change in plate's thermal behavior. To estimate its importance, we calculate next the characteristic heat conduction time across the plate $t_c \sim h_w^2 \rho_w c_w / k_w$, with k_w, ρ_w and c_w the thermal conductivity, density and heat capacity of the PMMA plate. On the other hand, the flame transit time and the experiment duration can be estimated as $t_f \sim \delta_L / S_L \sim D_T / S_L^2$ and $t_{exp} \sim L/S_L$, respectively. Using $k_w = 0.2$ W/m K, $\rho_w = 1200$ kg/m^3, $c_w = 1466$ J/kg K, $h_w = (10, 25)$ mm, we obtain $t_c \sim (880, 5500)$ s respectively. This time is much longer than the transit time $t_f \sim 10^{-4}$ s ($D_T = 20 \times 10^{-6}$ m^2/s and $S_L = 0.4$ m/s) or the experiment duration $t_{exp} \sim 1$ s and, therefore, we can anticipate that the thermal effect of reducing h_w in this range has a negligible influence on the propagation of the flame.

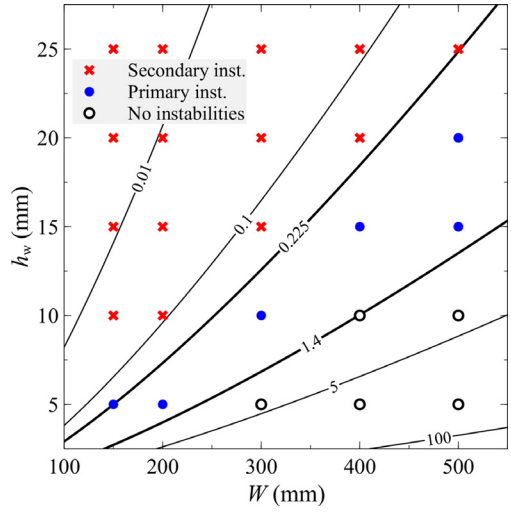

Fig. 7. Stability map in the $W - h_w$ parametric space. Red crosses and filled circles represent the cases in which the secondary and primary instabilities are observed, respectively. Empty circles are those cases in which no pressure oscillations were measured. The lines correspond to iso-contours of $\tilde{\Lambda} = \Lambda \Delta p$. The curve $\tilde{\Lambda} = \tilde{\Lambda}_{c,2} = 0.225$ identifies the onset of secondary instabilities while $\tilde{\Lambda} = \tilde{\Lambda}_{c,1} = 1.4$ depicts the boundary separating primary instabilities and no flame oscillations.

Further information can be obtained from the vertical displacement $d(t)$ in Fig. 3 (bottom), for the cases $h_w = 10$ and 25 mm. Shortly after ignition $t - t_0 \ll h/S_u$, with $S_u \sim 10$ m/s an estimation of the flame speed right after the ignition obtained from the experiments, it can be observed that the vertical displacement of the plate d is one order of magnitude smaller with $h_w = 25$ mm than with $h_w = 10$ mm. Correspondingly, the ignition-induced initial pressure increase observed in the pressure record is rapidly damped in the case $h_w = 10$ mm. This effect is a direct consequence of the small, but sufficient, volume expansion created by the deformation of the plate in z direction. As seen in Fig. 3, this feature determines the posterior evolution of the acoustic pressure wave, with an exponential increase of $p - p_a$ when $h_w = 25$ mm versus an almost negligible pressure variation when $h_w = 10$ mm.

Additional experiments changing W in the range of 150 to 500 mm provide the data to plot the stability map depicted in Fig. 7, where we summarize our experimental measurements indicating, with red crosses, the combination of parameters that cause secondary thermoacoustic instabilities. Dots are used to indicate primary oscillations (blue, filled) or steady propagation (black, empty) observed in the flame. In addition, the curves rep-

Please cite this article as: M. Rubio-Rubio, F. Veiga-López, D. Martínez-Ruiz et al., Suppression of thermoacoustic instabilities by flame-structure interaction, Proceedings of the Combustion Institute, https://doi.org/10.1016/j.proci.2022.07.165

resented in Fig. 7 correspond to iso-contours of $\tilde{\Lambda} = \Lambda\Delta p$, where $\Delta p = 100$ Pa is the value of the overpressure measured in our experiments. As suggested by Eq. (1), the parameter $\tilde{\Lambda}$ is proportional to the relative displacement d/h.

From the stability map included in Fig. 7 we identify the isolines $\tilde{\Lambda}_{c,2} = 0.225$ and $\tilde{\Lambda}_{c,1} = 1.4$ as the critical values separating the aforementioned oscillatory flame regimes, confirming the parametric dependence anticipated above by Eq. (1). Consequently, once the material of the upper plate and the parameters W and h_w are set, we can anticipate that thermoacoustic instabilities will be suppressed if $\tilde{\Lambda} > \tilde{\Lambda}_{c,1}$, primary oscillations are found when $\tilde{\Lambda}_{c,2} < \tilde{\Lambda} < \tilde{\Lambda}_{c,1}$ and secondary thermoacoustic oscillations when $\tilde{\Lambda} < \tilde{\Lambda}_{c,2}$. In terms of the relative displacement d/h, a volume expansion of the combustion chamber right after ignition of around 0.1% is enough to suppress the onset of thermoacoustic oscillations.

6. Conclusions

Our experimental measurements in a Hele–Shaw cell have shown a great influence of the structural rigidity on the thermo-acoustic stability of flames. When sufficiently rigid horizontal plates are used in the construction of the combustion chamber, large acoustic-induced flame oscillations are observed. On the contrary, if the top plate is substituted by compliant materials, flame oscillations disappear with the pressure acoustic waves dampening rapidly. The detailed analysis of both the accelerometer and pressure transducer indicates that the initial deformation of the plate determines the posterior evolution of both the acoustic pressure wave and the flame. The initial pressure rise generated by the gas ignition creates a vertical displacement of the plate that is one order of magnitude larger in thin plates. Thus, the volume expansion compensates for the increase of pressure observed in the ignition, reducing the amplitude of the flame oscillations caused by the acoustic pressure waves. The systematic modification of the width and thickness of the top plate points towards $\tilde{\Lambda} = \Lambda\Delta p$ as the parameter controlling the onset of undamped thermoacoustic instabilities, with Λ the material stiffness parameter and Δp the pressure rise during ignition. When $\tilde{\Lambda} > 1.4$, the initial vertical displacement of the plate is large enough to totally suppress flame thermoacoustic instabilities. Large pressure oscillations are avoided when $\tilde{\Lambda} > 0.225$, but small primary oscillations can still be observed during the propagation of the flame. Large secondary flame oscillations will be expected when $\tilde{\Lambda} < 0.225$.

Predicting the growth rate of pressure oscillations is crucial to design new control methods. An example of how the amplitude of pressure oscillations grows with time in our experiments is shown in Fig. 3. From a theoretical point of view, it is possible to anticipate the growth rate of the experiments by taking advantage of the disparity between the acoustic characteristic time $t_a \sim L/c$, with c representing the velocity of sound, and the flame propagation time $t_{exp} \sim L/S_L \gg t_a$. This feature simplifies the calculation by decoupling the computation of the acoustic field and the response of the flame [19]. The former can be computed using low order network models, but the later needs an accurate flame model capable of properly describing the unsteady non-linear behavior. Its determination, either numerically or experimentally is of central importance to correctly identify the growth rate and the amplitude saturation observed in Fig. 3. Moreover, such calculation should include the effect of the flexibility of the combustion chamber to take into account the new effect reported in this paper. Unfortunately, and regardless the intrinsic interest of the data that this approach can provide, this calculation falls out of the scope of this paper. In spite of this, our measurements bring the design of compliant combustion chambers to the spotlight as a novel method to control the onset of thermoacoustic instabilities. Therefore, this result might be used to extend the range of utilization of some fuels, like hydrogen, towards leaner mixtures where they give better burning efficiencies but are known to be acoustically unstable [6].

Declaration of Competing Interest

The authors declare that they have no known competing financial interests or personal relationships that could have appeared to influence the work reported in this paper.

Acknowledgments

This work was funded by the Agencia Estatal de Investigación of Spain under grants PID2019-108592RA-C43 and PID2019-108592RB-C41, and by the Regional Government of Madrid (Comunidad de Madrid-Spain) under the Multiannual Agreement with UC3M (H2SFE-CM-UC3M). The authors wish to thank the technical knowledge and assistance of David Díaz, Israel Pina and Manuel Santos in the design, construction and operation of the experimental setup. The assistance of Rubén Palomeque in the preparation of figure 6 is greatly acknowledged. We would also like to acknowledge Raúl San Miguel and Ramón Zaera for providing the values of E and ν of the PMMA plates.

Please cite this article as: M. Rubio-Rubio, F. Veiga-López, D. Martínez-Ruiz et al., Suppression of thermoacoustic instabilities by flame-structure interaction, Proceedings of the Combustion Institute, https://doi.org/10.1016/j.proci.2022.07.165

Appendix A

Table 1
Fundamental mode of the flame/pressure oscillation frequency f_f for the tested values of the plate's width W and thickness h_w. Gray cells indicate when secondary thermoacoustic instabilities are observed in the flame. Dash symbols - indicate when pressure oscillations where not detected.

h_w (mm)	W (mm)				
	150	200	300	400	500
25					114
20				104	106
15	118	117	107	99	100
10	116	109	97	–	–
5	106	97	–	–	–

Table 2
Natural frequency in the first deformation mode $f_{1,1}$ (Hz) of a PMMA plate of width W and thickness h_w, obtained under the effect of a constant load.

h_w (mm)	W (mm)				
	150	200	300	400	500
25	1346.9	810.2	380.8	219.5	142.7
20	1138.9	671.4	310.0	177.4	114.9
15	896.4	518.6	235.8	134.1	86.7
10	620.8	353.6	158.8	90.0	58.0
5	318.6	179.5	80.0	45.2	29.1

Table 3
Second deformation mode natural frequency $f_{1,2}$ (Hz) of a PMMA plate of width W and thickness h_w, obtained under the effect of a constant load.

h_w (mm)	W (mm)				
	150	200	300	400	500
25	1364.9	830.0	403.2	243.9	168.8
20	1154.7	688.2	328.5	197.3	136.1
15	909.3	531.9	250.0	149.3	102.8
10	630.0	362.8	168.5	100.2	68.8
5	323.3	184.2	84.9	50.3	34.5

Supplementary material

Videos of Figs. 2 and 6 are provided as supplementary material.

Supplementary material associated with this article can be found, in the online version, at doi:10.1016/j.proci.2022.07.165

References

[1] J. Gross, X. Pan, P. Ronney, Flame propagation at low lewis number in narrow slots, in: Western States Section of the Combustion Institute Spring Technical Meeting, 2014, pp. 320–326.
[2] M.M. Alexeev, O.Y. Semenov, S.E. Yakush, Experimental study on cellular premixed propane flames in a narrow gap between parallel plates, Combust. Sci. Technol. 191 (2019) 1256–1275.
[3] E.A. Sarraf, C. Almarcha, J. Quinard, B. Radisson, B. Denet, Quantitative analysis of flame instabilities in a Hele–Shaw burner, Flow Turbul. Combut. 101 (2018) 851–868.
[4] S. Shen, J. Wongwiwat, P. Ronney, Flame propagation in quasi-2d channels: Stability, rates and scaling, AIAA Scitech 2019 Forum, 2019.
[5] F. Veiga-López, D. Martínez-Ruiz, E. Fernández–Tarrazo, M. Sánchez-Sanz, Experimental analysis of oscillatory premixed flames in a Hele–Shaw cell propagating towards a closed end, Combust. Flame 201 (2019) 1–11.
[6] F. Veiga-López, D. Martínez-Ruiz, M. Kuznetsov, M. Sánchez-Sanz, Thermoacoustic analysis of lean premixed hydrogen flames in narrow vertical channels, Fuel 278 (2020) 118212.
[7] D. Martínez-Ruiz, F.V. López, M. Sánchez-Sanz, Vessel confinement contributions to thermo-acoustic instabilities of premixed flames, Bulletin of the American Physical Society, vol. 63, 2018.
[8] D. Martínez-Ruiz, F. Veiga-López, M. Sánchez-Sanz, Premixed-flame oscillations in narrow channels, Phys. Rev. Fluids 4 (2019) 100503.
[9] G. Searby, Acoustic instability in premixed flames, Combust. Sci. Technol. 81 (1992) 221–231.
[10] B. Radisson, J. Piketty-Moine, C. Almarcha, Coupling of vibro-acoustic waves with premixed flame, Phys. Rev. Fluids 4 (2019) 121201.
[11] Y. Liu, J. Du, L. Cheng, Thermoacoustic modal instability and its suppression with locally resonant flexible membranes, Combust. Flame 237 (2022) 111859.
[12] T.C. Lieuwen, V. Yang, Combustion Instabilities in Gas Turbine Engines: Operational Experience, Fundamental Mechanisms, and Modeling, American Institute of Aeronautics and Astronautics, 2005.
[13] A.K. Pozarlik, J.B.W. Kok, Fluid-structure interaction in combustion system of a gas turbineeffect of liner vibrations, J. Eng. Gas Turb. Power 136 (2014) 091502.
[14] L.D. Landau, E.M. Lifshitz, Fluid Mechanics: Course of Theoretical Physics, vol. 6, Elsevier, 2013.
[15] A.W. Leissa, Vibration of Plates, Technical Report, National Aeronautics and Space Administration, 1969.
[16] S. Timoshenko, S. Woinowsky-Krieger, Theory of Plates and Shells, Engineering Mechanics Series, McGraw-Hill, 1959.
[17] A. Crespo Martínez, Mecánica de Fluidos, Editorial Paraninfo, 2006.
[18] E. Flores-Montoya, V. Muntean, M. Sánchez-Sanz, D. Martínez-Ruiz, Non-adiabatic modulation of premixed-flame thermoacoustic frequencies in slender tubes, J. Fluid Mech. 0 (2022) A1.
[19] X. Han, J. Li, A.S. Morgans, Prediction of combustion instability limit cycle oscillations by combining flame describing function simulations with a thermoacoustic network model, Combust. Flame 162 (10) (2015) 3632–3647.

Please cite this article as: M. Rubio-Rubio, F. Veiga-López, D. Martínez-Ruiz et al., Suppression of thermoacoustic instabilities by flame-structure interaction, Proceedings of the Combustion Institute, https://doi.org/10.1016/j.proci.2022.07.165